POLITECNICO DI TORINO
Repository ISTITUZIONALE

Magnet shape optimization of surface-mounted permanent magnet synchronous machine through FEA method

(Article begins on next page)

04 August 2020

MAGNET SHAPE OPTIMIZATION OF SURFACE-MOUNTED PERMANENT MAGNET SYNCHRONOUS MACHINE THROUGH FEA METHOD

Chao LU and Gianmario PELLEGRINO
Politecnico di Torino
Department of Energy, Turin, Italy, 10129
chao.lu@polito.it   gianmario.pellegrino@polito.it

Abstract: This work analyzes the effects of permanent magnet shape on the performance of surface-mounted permanent magnet (SPM) machine, including average torque, cogging torque, magnet volume and de-magnetization limit. Analytical expressions are introduced to obtain the relationship between magnet shape and torque behaviors. Secondly, a multi-objective Differential Evolution (MODE) algorithm is used to get the best tradeoff model between torque performances. An automatic design process via MODE for SPM motor with magnet shaping is introduced. All the models are validated by Finite Element Analysis (FEA).

Key words: Magnet shape, Cogging torque, Multi-objective optimization

1. Introduction

Thanks to their high efficiency, high torque density, and good dynamic performance, permanent magnet synchronous motors (PMSMs) have been widely utilized in industrial applications, electric vehicles and aerospace over last several decades. Among PMSMs, surface-mounted permanent magnet (SPM) motors are popular due to their simple configuration, compared to Interior permanent magnet (IPM) motors [1].

Nonetheless, the cogging torque of SPM motors, which results from interaction between permanent magnet (PM) edge and stator slot openings causing vibration and noise, is a significant issue for high performance requirements [2]. Many methods have been developed for reducing cogging torque [3], for example, rotor skewing, magnet shifting or shaping, applying notches in stator teeth, etc. Each method has its own merits and drawbacks. In terms of skewing, although it effectively diminishes cogging torque, it also reduces the torque output of the machine and increases the manufacturing cost [4]. Similarly, magnet shaping can decrease the interaction between magnet and stator teeth, at the risk of reducing the fundamental airgap flux density, and therefore average output torque.

Several optimization algorithms have been used in machine design process to achieve optimal torque, power or field weakening capability in recent years [5]. Among multi-objective optimization algorithms, multi-objective differential evolution (MODE) is one of the well-accepted methodologies for motor design optimization [6]. For example, torque and flux weakening capability of a concentrated-winding SPM machine for traction application were Pareto-optimized in [7].

This research deals with analytical calculation of SPM motors cogging torque, when magnet shaping is applied. Based on that, this paper investigates the trade-off between average torque and cogging torque performance using a constrained stator geometry and MODE optimization. Demagnetization of PMs and volume (i.e. cost) of PMs are also considered in the study. In turn, the paper formulates an automatic design process for SPM motors with magnet shaping, validated by Finite Element Analysis (FEA).

2. Torque model

One pole of an SPM rotor with shaped magnets is reported in Fig.1. The outer profile of the PM is circular and follows the set of parameters defined in the figure. l_m is the maximum magnet length at the center of the pole, r is the rotor iron radius, β is the magnet length at the magnet edge, in p.u. of l_m. When β equals to 1, the magnet length is uniform. α_m is the magnet angular span, ξ is the rotor angular coordinate, starting from the magnet center, $g(\xi)$ is the airgap length function of ξ and r_c is the radius of the outer rounded magnet profile. After defining the magnet parameters (α_m, l_m and β), the magnet length distribution $l_m(\xi)$, r_c and central position O' of rounded profile are calculated.

Assuming that the current vector having amplitude i_0 is controlled on the q axis, the torque output is:

$$T = \frac{3}{2} \cdot p \cdot \lambda_m \cdot i_0 \qquad (1)$$

Where p is the number of pole pairs, λ_m is magnet flux linkage and i_0 is the motor maximum current. The magnet flux linkage λ_m is evaluated considering the fundamental component of the airgap flux density and neglecting higher order harmonics:

$$\lambda_m = D_{is}L \cdot \frac{k_w N_s}{p} \cdot B_{g1} \qquad (2)$$

Where L is the stack length, N_s is the number of turns per phase, k_w is the winding factor, D_{is} is the stator inner diameter and B_{g1} is the peak of fundamental airgap flux density.
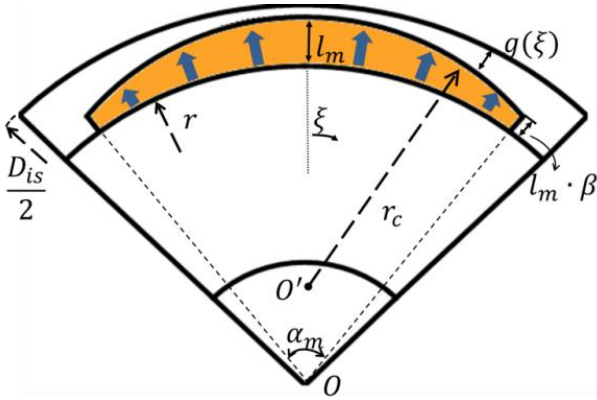

Fig. 1. Definition of design parameters for SPM motors with circular PM shape

2.1 Airgap flux density distribution

Assuming that the airgap flux is radial and that the cross sectional areas of PMs and airgap are equal, for a slotless machine, it is obtained that,

$$B_g(\xi) \cong B_m(\xi) = \frac{l_m(\xi)/g(\xi)}{l_m(\xi)/g(\xi)+k_c \cdot \mu_r} \cdot B_r \qquad (3)$$

Here $B_m(\xi)$ is the magnet flux density function, k_c is the Carter coefficient, and μ_r is the relative permeability of the magnet, and B_r is the magnet remanent flux density.

The magnet length function $l_m(\xi)$ is not only dependent on ξ, it also relies on the magnet length ratio β at magnet edge. It is can be seen that while β increases, $B_g(\xi)$ will also rises, thus making B_{g1} increase. The limitation of β will be discussed in next section. Based on the magnet parameters input (l_m, α_m and β), the radius of rounded magnet shape r_c and $l_m(\xi)$ can be achieved as,

$$r_c = \frac{\left(2r^2+2l_m r(\beta+1)\right)\left(1-\cos\frac{\alpha_m}{2}\right)+(\beta^2+1-2\beta\cos\frac{\alpha_m}{2})l_m^2}{2(r\left(1-\cos\frac{\alpha_m}{2}\right)+l_m(1-\beta\cos\frac{\alpha_m}{2}))} \qquad (4)$$

$$l_m(\xi) = (r + l_m - r_c)\cos\xi - r + \sqrt{r_c^2 - ((r+l_m)sin\xi - r_c sin\xi)^2} \qquad (5)$$

The relationship among stator inner diameter D_{is}, $l_m(\xi)$ and $g(\xi)$ is given,

$$l_m(\xi) + g(\xi) + r = D_{is}/2 \qquad (6)$$

Then substituting (5) into (6), the airgap length is then calculated as,

$$g(\xi) = D_{is}/2 - (r + l_m - r_c)\cos\xi - \sqrt{r_c^2 - ((r+l_m)sin\xi - r_c sin\xi)^2} \qquad (7)$$

Combining equations (3) to (7), the airgap flux density expression $B_g(\xi)$ is calculated as,

$$B_g(\xi) = ((r + l_m - r_c)\cos\xi - r + \sqrt{r_c^2 - ((r+l_m)sin\xi - r_c sin\xi)^2}) \cdot B_r /$$
$$((1-k_c\mu_r)(r+l_m-r_c)\cos\xi + (1-k_c\mu_r)\sqrt{r_c^2 - ((r+l_m)sin\xi - r_c sin\xi)^2}$$
$$-r + \frac{k_c \cdot \mu_r D_{is}}{2}) \qquad (8)$$

Three cases of airgap flux density distribution $B_g(\xi)$ waveforms are reported in Fig. 2. The analytical results are presented in continuous lines and the circle marked points represent the FEA results. It can be seen that the analytical results agree with the FEA results along with the PM areas. Nonetheless, influenced by fringing effect, in the regions without PMs, the flux density cannot vanish, as indicated by the FEA results. The proposed mathematical model (8) assumes the airgap flux density to be zero off the magnet pole, with minor effect on torque and power factor prediction.

The fundamental component's amplitude B_{g1} is obtained by Fourier transform of the analytical flux density distribution $B_g(\xi)$. Then λ_m is calculated by (2). Table 1 summarizes the difference between

analytical results and FEA results on λ_m. The matching of the results is reasonably good for all considered values of the parameter β.
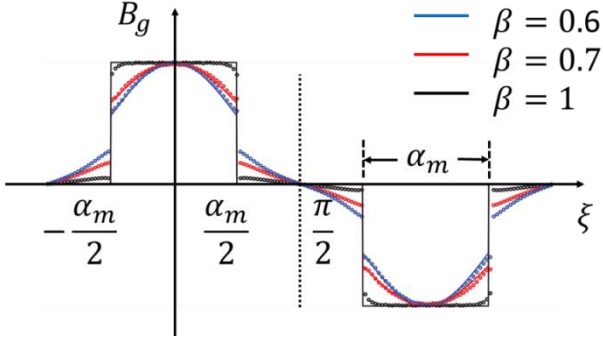

Fig. 2. Airgap flux density distribution of a slotless motor, analytical results: continuous lines; FEA results: circle marked

Table 1 Difference between analytical and FEA results

$\begin{array}{l} l_m = 5\ mm \\ g_{min} = 1\ mm \\ \alpha_m = 150° \end{array}$	β	0.6	0.7	1
B_{g1} [T]	Analytical	1.02	1.05	1.15
	FEA	1.04	1.06	1.13
	Error %	-2	-1	+1.7
λ_m [Wb-t]	Analytical	0.48	0.50	0.55
	FEA	0.49	0.50	0.54
	Error %	-2	0	+1.9

2.2 Cogging torque model

Cogging torque is caused by the interaction between the PMs fixed on the rotor surface and stator slots. While the PMs are rotating, the magnetic energy varies with rotor position angle θ. The cogging torque can be calculated based on energy derivative method,

$$T_{cog}(\theta) = -\frac{\partial W_0}{\partial \theta} \qquad (9)$$

Where W_0 is the total magnetic energy stored in the motor at open circuit conditions (zero current), function of the rotor position only. Since the magnetic energy stored in the iron and PMs is negligible compared with that one stored in the airgap, only the airgap volume and corresponding flux density distribution will be considered for the determination of the motor magnetic energy. At zero current, the magnetic energy is expressed as [8]

$$W_0(\theta) = \frac{1}{2\mu_0} \int_V B_{g0}\, dV \qquad (10)$$

The airgap flux density distribution at zero current B_{g0} can be achieved from the product of slotless machine distribution $B_g(\xi, \theta)$ and airgap permeance function $G(\xi)$, accounting for the slot opening effect.

$$B_{g0} = B_g(\xi, \theta) \cdot G(\xi) \qquad (11)$$

From (9), (10) and (11), the cogging torque expression can be derived as,

$$T_{cog}(\theta) = \frac{\pi L}{4\mu_0}\left(\left(r + l_m(\xi)\right)^2 - \left(\frac{D_{is}}{2}\right)^2\right) \cdot$$

$$\frac{\partial}{\partial \theta} \int_0^{2\pi} B_g^2(\xi, \theta) \cdot G^2(\xi)\, d\xi \qquad (12)$$

Where μ_0 is the air permeability. If $G^2(\xi)$ and $B_g^2(\xi, \theta)$ are expressed as Fourier series, (12) can be transformed as:

$$T_{cog}(\theta) = \frac{\pi L k}{4\mu_0}\left(\left(r + l_m(\xi)\right)^2 - \left(\frac{D_{is}}{2}\right)^2\right) \cdot$$

$$\sum_{n=1}^{\infty} n G_{a_n k} B_{a_n k} \sin(nk\theta) \qquad (13)$$

In the equation, k is the least common multiple (LCM) of stator slot number Q_s and $2p$, and n is the harmonic order. The equation presents that the cogging torque relates to the magnet length $l_m(\xi)$, coefficients $G_{a_n k}$ and $B_{a_n k}$, and k. The cross sectional view of a simplified stator slot is shown in Fig. 3. The Fourier coefficients $G_{a_n k}$ of the airgap relative permeance can be calculated as suggested in [9],

$$G_{a_n k} = \frac{Q_s}{\pi}\left(\int_{-\frac{\pi}{Q_s}}^{-\frac{d_0}{2}} \cos(nk\theta)d\theta + \int_{\frac{d_0}{2}}^{\frac{\pi}{Q_s}} \cos(nk\theta)d\theta\right)$$

$$= -\frac{Q_s}{\pi}\frac{2}{nk}\sin(\frac{d_0}{2} \cdot nk) \qquad (14)$$

Equation (14) shows that $G_{a_n k}$ relates to the slot opening d_0 and it is independent upon magnet shape.
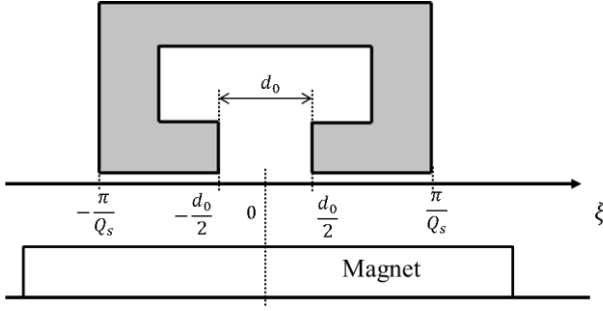
Fig. 3. Stator slot cross-section view

The other Fourier coefficient B_{a_nk} is calculated as,

$$B_{a_nk} = \frac{4p}{\pi} \int_0^{\frac{\alpha_m}{2p}} B_g^{\,2}(\xi) \cos(nk\xi)\, d\xi \qquad (15)$$

It is can be seen that the magnet shape parameters α_m, β and l_m are relevant to B_{a_nk}. Substituting (14) and (15) into (13), cogging torque expression can be obtained as,

$$T_{cog}(\theta) = \frac{\pi L k}{4\mu_0}\left(\left(r + l_m(\xi)\right)^2 - R^2\right) \cdot$$

$$\sum_{n=1}^{\infty}\left[-\frac{Q_s}{\pi}\frac{2}{k}\sin\left(\frac{d_0}{2}nk\right)\frac{4p}{\pi}\sin(nk\theta) \cdot \right.$$
$$\left. \int_0^{\frac{\alpha_m}{2p}} B_g^{\,2}(\xi) \cos(nk\xi)\, d\xi\right] \qquad (16)$$

In this research, the stator geometry and slot and pole pair combination are fixed: $Q_s = 36, p = 3$, therefore $k = 36$ (see Table 2). The influence of magnet shape parameters α_m, β and l_m on cogging torque according to (16) are reported in Fig. 4. The cogging torque results are measured as peak-peak value. It can be seen that $\alpha_m = 150°$ has the strongest anti-cogging effect, as expectable with this number of slots [8], and that further reduction to cogging can be achieved by limiting β when α_m and l_m are invariant. Moreover, each β relates to an optimal α_m, which is an original contribution of this analysis. For example, for $\beta < 0.4$ the value $\alpha_m = 150°$ is no longer the optimal magnet span.
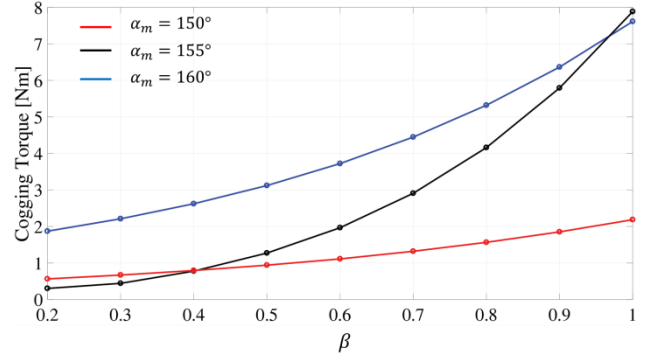

Fig. 4. Influence of α_m and β on peak-peak cogging torque, $l_m(\xi = 0) = 5mm$, $g(\xi = 0) = 1mm$

3. Torque and cogging optimization

The main motor ratings of the selected design example are reported in Table 2. MODE and FEA methods are utilized to optimize PM shape giving optimal λ_m and T_{cog} at open load condition. By applying (1), the torque output is obtained from the product of λ_m and i_0. The optimization inputs are: l_m, α_m and β. Other cost functions considered off-line after the optimization are the distance from the demagnetization limit and the mass of the PMs. The procedure of optimization process is shown in Fig. 5.
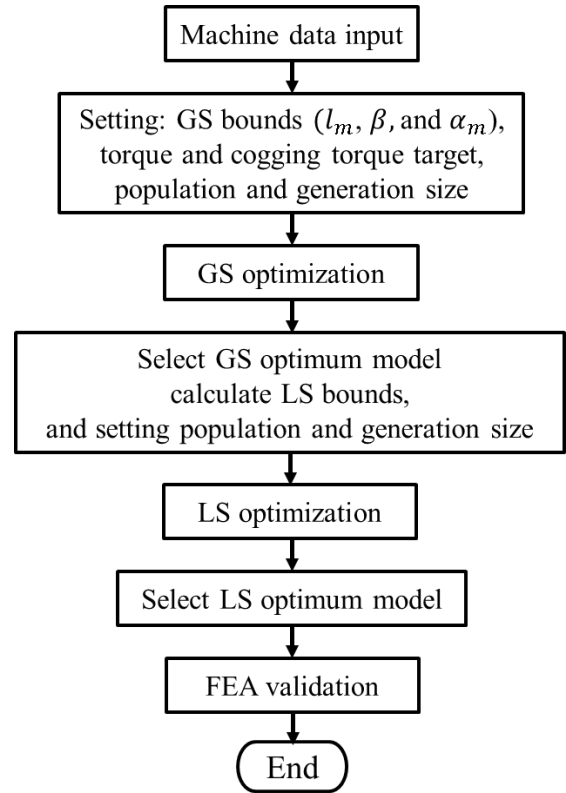

Fig. 5. Flowchart of optimization procedure

Table 2 Main parameters of target machine

Parameters	Values	Units
Number of slots	36	
Pole pairs	3	
Stator inner diameter	120	mm
Stator outer diameter	175	mm
Stack length	110	mm
Minimum airgap length	1	mm
Slot opening	0.3	
Maximum current	26	A
Maximum speed	1000	rpm
Number of turns per phase	120	
Torque target	56	Nm
Peak cogging torque limit	1	Nm

3.1 Demagnetization and magnet edge length limitation

To prevent fracture in manufacturing process, the PM ends should not be too thin. Besides the manufacturing issues, the PMs must be protected against demagnetization by having adequate minimum length βl_m. The maximum armature magnetoforce (mmf) per pole is defined as [10],

$$F_{p1} = \frac{3}{2}\frac{4}{\pi}\frac{k_w N_s}{2p} i_0 \tag{17}$$

It is assumed that all of the mmf drop occurs over the air gap and saturation of stator iron is neglected. The air gap flux density produced by armature current alone is maximum at the magnet's edges, calculated as,

$$B_{g,S} = \frac{F_{p1}\mu_0}{g} = \frac{3}{2}\frac{4}{\pi}\frac{\mu_0 k_w N_s}{2p(l_m(\xi=0)+\mu_r k_c g(\xi=0))} i_0 \tag{18}$$

To prevent demagnetization at maximum current condition, the flux density at PM edge must be equal or larger than minimum allowed flux density in the magnet B_d (knee point of the magnet characteristic). Therefore, the flux density $B_m(\xi = \frac{\alpha_m}{2})$ at open load condition should be not less than the sum of $B_{g,S}$ and B_d, thus:

$$B_m(\xi = \frac{\alpha_m}{2}) \geq B_{g,s} + B_d \tag{19}$$

Corresponds to (19), B-H curve on the relationship among $B_m(\xi = \frac{\alpha_m}{2})$, $B_{g,S}$ and B_d is shown in Fig. 6. The relationship among maximum allowed current, l_m and β is reported in Fig. 7. It illustrates that the maximum current is in

proportional to the magnet length ratio β when l_m is fixed. In this study, B_d is chosen as $0.1T$ (BMN-42SH at 80℃). Then, from (3), (18) and (19), the minimum length at magnet edge is achieved as 1.7 mm, i.e. $\beta = 0.24$ while $l_m(\xi = 0) = 7\ mm$.
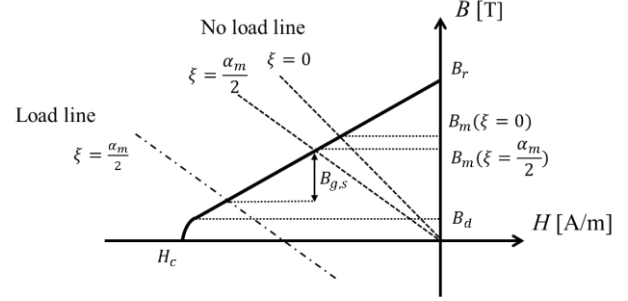

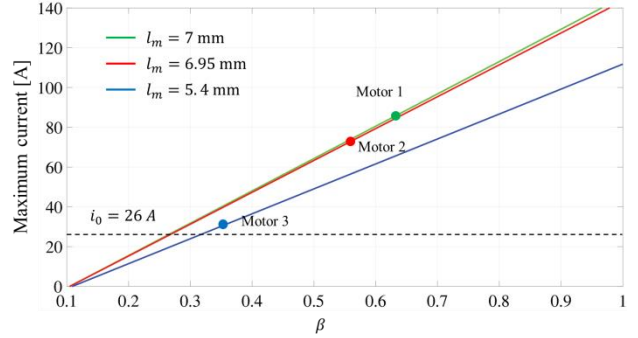Fig. 6. Operating point determination with demagnetization limit

Fig. 7. Relationship among β, l_m and maximum allowed current

3.2 Optimal magnet span range

For magnets having constant length the magnet span α_m giving minimum cogging torque is as [8],

$$\frac{\alpha_m}{\tau_p} = \frac{N-m_1}{N} + m_2 \tag{20}$$

Where $N = k/2p$ ($N = 6$ in the reported example), m_1 is an integer from 1 to $(N-1)$, τ_p is the pole pitch. Due to the fringing PM flux entering into the slot side, additional factor m_2 should be taken into account, which ranges from 0.01 to 0.03 [11]. The formula is valid for magnets having uniform thickness. In this paper, the airgap thickness is gradually increasing from pole center to PM edge, making the mutual effect between PM edge and slots less acute than that in uniform thickness PM case. Based on that, in order to achieve more possible solutions, m_2 has been increased to 0.05. Since larger α_m generate higher torque according to (5) and (8), it is convenient to set $m_1 = 1$. In this study, the range of PM span is set as $0.83\tau_p$ to $0.88\tau_p$.

After defining the bounds of PM shape, the MODE procedure will automatically optimize the torque and cogging torque performance.

3.3 Result of optimization

As mentioned beforehand, the stator geometry in this study is fixed. According to [5], MODE is more efficient to get desired results in terms of the number of machine candidates. The bounds setting of magnet parameters are shown in Table 3.

A two-stage optimization procedure is used here to save the running time which consists of first step called global search (GS) and a refined step called local search (LS). This approach was first suggested in [6]. During the GS process, 10000 candidates are involved (100 individuals in one population over 100 generations). Each candidate is evaluated by 31 FEA simulations for 31 rotor positions distributed evenly over one slot pitch. Then cogging torque is defined as the difference between maximum and minimum torque values. λ_m is the mean flux linkage value along with d axis of total 31 simulations. Then the maximum torque capability is calculated by (1) and reported as a negative value. After 16-hour parallel computing processing in a standard desktop computer (*Intel i7*, 4-core, 16 GB RAM), the Pareto front is obtained. One promising solution is selected as the base design for the subsequent LS stage. The search bounds of the LS optimization are $\pm$ 5% of base model data input. Then another 200 refined candidates are evaluated in 30 minutes. The final Pareto front consists of both GS and LS stage is reported in Fig. 8.
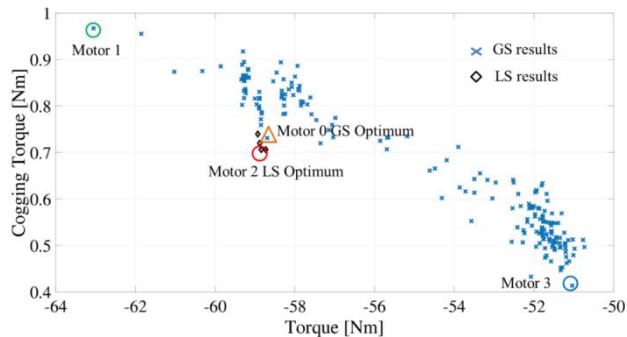

Fig. 8. Pareto front of both GS and LS stages

The optimization result consists of 208 motors from the evolution process. From Fig. 8, it is reported that the lowest cogging torque is around 0.4 Nm in this research. However the motor with lowest cogging torque is not able to generate adequate

maximum torque (blue circle, Motor 3). Conversely, the one can produce highest torque has a worst cogging torque situation (green circle, Motor 1). The motor located at left bottom of Pareto front (red circle, Motor 2) is the one with best tradeoff between cogging torque and torque producing capability. The cross-sections of three motors are shown in Fig. 9 with their relative magnet parameters.

Table 3 Limit of search space for optimization

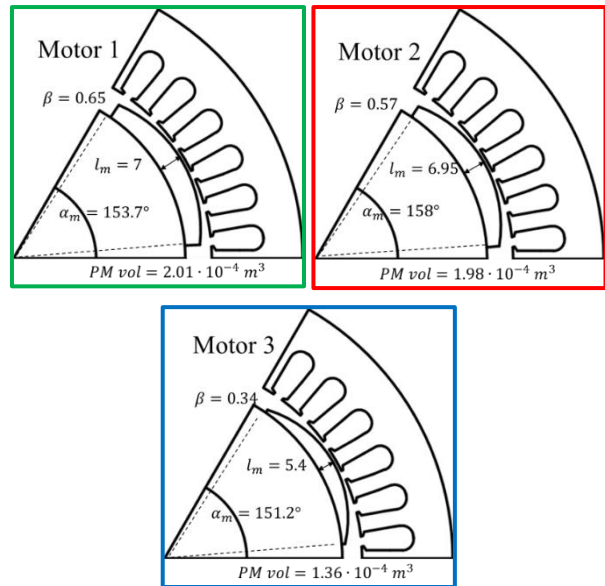| Magnet parameter	l_m	β	α_m
Bounds (GS)	[5, 7]	[0.24, 1]	[150, 159]
GS-optimum (Motor 0)	6.89	0.55	155.7
Bounds (LS)	[6.54,7]	[0.52, 0.57]	[150, 159]
LS-optimum (Motor 2)	6.95	0.57	158
Units	mm	p.u.	elt. degree

Fig. 9. Three different motor cross-sections from Pareto front

The detailed cogging torque waveforms of three motors over two slot pitches are presented in Fig. 10. The zero rotor position is defined as the line where the PM center aligned with the tooth center as the same position shown in Fig. 9. Although the cogging torque performance of Motor 3 is the best solution among the Pareto front, the torque production is considerably lower than others. The red model is chosen as the optimal solution to be a prototype since it can achieve the maximum torque target (56 Nm) with relatively low cogging torque. The torque

waveforms for the three motors over an entire period under maximum current condition are presented in Fig. 11. The average torque outputs from FEA are matched with the analytical results obtained from (1). Moreover, it also illustrates that the torque ripples of the three motors have the same trend of their cogging torque results. The torque ripple has been reduced while the edge length of magnet becomes shorter (from Motor 1 to Motor 3). Considering the cost, a larger amount of magnets is used in Motor 1. Compared with Motor 1, Motor 2 is also the cost-optimal one, shown in Fig. 9.
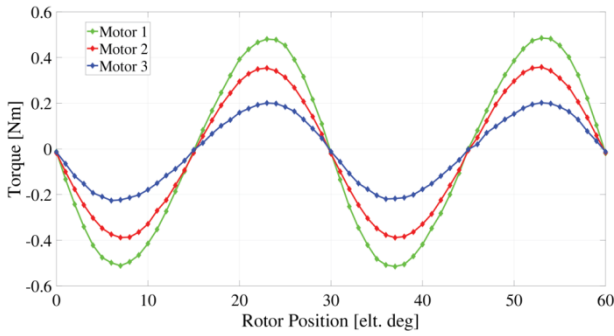
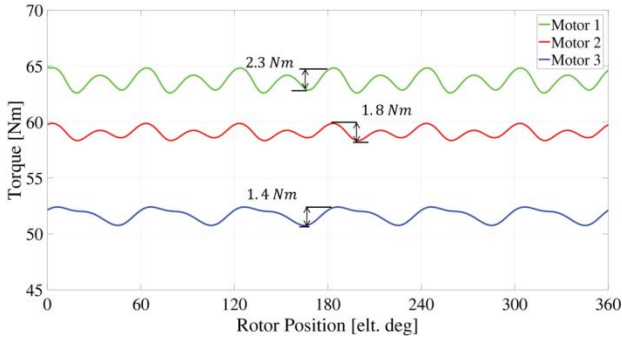

Fig. 10. Cogging torque waveforms of three motors

Fig. 11. Torque waveforms of the three motors

Table 4 Analytical and FEA results comparison on magnet edge

		$B_m(\xi = \frac{\alpha_m}{2})$ [T]	$B_{g,s}$ [T]	B_{min} [T]
Motor 1	Analytical	0.63	0.23	0.4
	FEA	0.65	-	0.49
Motor 2	Analytical	0.55	0.2	0.35
	FEA	0.61	-	0.46
Motor 3	Analytical	0.33	0.14	0.19
	FEA	0.39	-	0.31

Considering the demagnetization limit, the minimum flux density on PM edge from analytical and FEA results of the three motors are reported in Table 4. The FEA results on B_{min} are higher than those from analytical calculation since the current is not applied along q axis. The FEA results present that the PMs are prevented from demagnetizing risk.

4. Conclusion

This paper presented a design procedure to optimize the PM shape of rounded SPM motors to find an optima tradeoff between torque and cogging torque behaviors. Both torque and cogging torque calculation through magnet shaping method is analyzed. Dependent on demagnetization limit and optimal magnet span calculation, the magnet bounds in optimization process are obtained. The cogging torque and maximum torque waveforms of three different motors on Pareto front are shown, which is obtained by MODE optimization and FEA simulations. One optimum motor is selected as the best trade-off machine among PM volume, torque and cogging torque behaviors.

References

1. Pellegrino, G., Vagati, A., Guglielmi, P., and Boazzo, B.: *Performance Comparison Between Surface-Mounted and Interior PM Motor Drives for Electric Vehicle Application.* in IEEE Transactions on Industrial Electronics, vol. 59, no. 2, pp. 803-811, Feb. 2012.

2. Islam, R., Husain, I., Fardoun, A., and McLaughlin, K.: *Permanent-Magnet Synchronous Motor Magnet Designs With Skewing for Torque Ripple and Cogging Torque Reduction.* in IEEE Transactions on Industry Applications, vol. 45, no. 1, pp. 152-160, Jan.-Feb. 2009.

3. Zhu, Z. Q., and Howe, D.: *Influence of design parameters on cogging torque in permanent magnet machines.* in IEEE Transactions on Energy Conversion, vol. 15, no. 4, pp. 407-412, Dec 2000.

4. Jahns, T. M., and Soong, W. L.: *Pulsating torque minimization techniques for permanent magnet AC motor drives-a review.* in IEEE Transactions on Industrial Electronics, vol. 43, no. 2, pp. 321-330, Apr 1996.

5. Duan, Y., and Ionel, D. M.: *A Review of Recent Developments in Electrical Machine Design Optimization Methods With a Permanent-*

Magnet Synchronous Motor Benchmark Study. in IEEE Transactions on Industry Applications, vol. 49, no. 3, pp. 1268-1275, May-June 2013.

6. Pellegrino, G., Cupertino, F., and Gerada, C.: *Automatic Design of Synchronous Reluctance Motors Focusing on Barrier Shape Optimization.* in IEEE Transactions on Industry Applications*,* vol. 51, no. 2, pp. 1465-1474, March-April 2015.

7. Lu, C., Ferrari, S., and Pellegrino, G.: *Two Design Procedures for PM Synchronous Machines for Electric Powertrains.* in IEEE Transactions on Transportation Electrification*,* vol. 3, no. 1, pp. 98-107, March 2017.

8. Lateb, R., Takorabet, N., and Meibody-Tabar, F.: *Effect of magnet segmentation on the cogging torque in surface-mounted permanent-magnet motors.* in IEEE Transactions on

Magnetics*,* vol. 42, no. 3, pp. 442-445, March 2006.

9. Zhu, L., Jiang, S. Z., Zhu, Z. Q., and Chan, C. C.: *Analytical Methods for Minimizing Cogging Torque in Permanent-Magnet Machines.* in IEEE Transactions on Magnetics*,* vol. 45, no. 4, pp. 2023-2031, April 2009.

10. Lipo, T. A.: *Introduction to AC machine design.* Wisconsin Power Electronics Research Center, University of Wisconsin, 2004.

11. Zarko, D., Ban, D., and Lipo, T. A.: *Analytical Solution for Cogging Torque in Surface Permanent-Magnet Motors Using Conformal Mapping.* in IEEE Transactions on Magnetics, vol. 44, no. 1, pp. 52-65, Jan. 2008.